2011

Temperature effects in terahertz step well quantum cascade structures with diagonal optical transition

Freeman, Will; Karunasiri, Gamani

SPIE

Freeman, Will, and Gamani Karunasiri. "Temperature effects in terahertz step well quantum cascade structures with diagonal optical transitions." Terahertz Emitters, Receivers, and Applications II. Vol. 8119. International Society for Optics and Photonics, 2011.

http://hdl.handle.net/10945/60311

Temperature effects in terahertz step well quantum cascade structures with diagonal optical transitions

Will Freeman, Gamani Karunasiri

Will Freeman, Gamani Karunasiri, "Temperature effects in terahertz step well quantum cascade structures with diagonal optical transitions," Proc. SPIE 8119, Terahertz Emitters, Receivers, and Applications II, 81190A (7 September 2011); doi: 10.1117/12.894223

SPIE.

Event: SPIE Photonic Devices + Applications, 2011, San Diego, California, United States

Temperature effects in terahertz step well quantum cascade structures with diagonal optical transitions

Will Freeman[a] and Gamani Karunasiri[b]
[a]Physics Division, Naval Air Warfare Center, China Lake, CA 93555, USA
[b]Physics Department, Naval Postgraduate School, Monterey, CA 93943, USA

ABSTRACT

Temperature effects in terahertz (THz) step well quantum cascade (QC) structures are investigated. Step well QC structures with diagonal optical transitions that use fast intrawell electron-longitudinal optical (LO) phonon scattering for depopulation are considered. A density matrix method is used to model the electron transport coherence and is incorporated into the Monte Carlo simulations of these structures. A phenomenological dephasing time is also included. The influence of the lattice temperature on the population inversion is modeled and the effects due to gain spectral broadening are also considered. Optical gain greater than typical waveguide resonator thresholds are estimated out to $T \sim 200$ K.

Keywords: THz, quantum cascade, step well, diagonal optical transition, lattice temperature, optical gain spectra, electron transport, density matrix, coherence.

1. INTRODUCTION

THz QC lasers have continuously improved since their inception[1] in terms of both output power and device operating temperature. Several QC configurations[2] for the active region have been used and proposed. Milliwatt power levels have been achieved, but the maximum operating temperature so far is still below 200 K without employing a magnetic field.[3] QC lasers have not only attracted the attention of experimentalists but also the attention of theoreticians as well. A number of techniques to varying degrees of accuracy have been developed and used to model the electron transport within these devices.[4-19] Some have used the nonequilibrium Green's function approach[6,8,11-15] and efforts to model the optical gain linewidth temperature dependence have been made.[12] But it has been argued that these techniques should better predict the temperature dependence of the linewidth. Another approach that has been reported used a simplified density matrix method to estimate the gain spectra at cryogenic temperatures in so-called resonant phonon structures (where the lower lasing state is resonantly tunneled).[17,18] Approximations were made where the nonequilibrium electron distributions were neglected and only the states within a periodic section needed for the laser action were included in the analysis. Other approximations have been made such as assuming a unity injection efficiency and neglecting back-scatter rates.[17] Under such approximations, the density matrix method reduces to the solution of simple rate equations while at the same time conveniently providing a straight forward way to include transport coherence and dephasing. Some of the results have suggested a double peaked gain spectra as a plausible way to explain certain experimental observations. However, because the nonequilibrium electron distributions were not solved and not all states within a periodic section were included, accurate temperature dependence of QC structures would seemingly be difficult to estimate using such an approach. Nonetheless, these types of modeling techniques are certainly useful for predicting transport properties in QC devices.

Recently, step well structures that feature a multi-step one-well structure and a principally two-well structure were proposed and the electron transport properties were modeled using a density matrix Monte Carlo approach at the cryogenic temperature of 25 K.[19] The two structures that were analyzed are shown in Fig. 1. Both structures have a diagonal optical transition, which is a sideways photon assisted tunneling transition, between the upper and the lower lasing states $|2\rangle \rightarrow |1\rangle$. The lower lasing state is intended to be rapidly depopulated via fast intrawell LO phonon scattering to the lower ground state $|1\rangle \rightarrow |0\rangle$ (scattering rate lifetime $\tau_{LO,1\rightarrow 0} \sim 0.2$ psec) since $\Delta E_{1\text{-}0} \approx \hbar\omega_{LO}$ (~ 36 meV in GaAs). These structures attempt to utilize the advantages a step well structure can offer (good injection selectivity and

Terahertz Emitters, Receivers, and Applications II, edited by Manijeh Razeghi, Nicolas Péré-Laperne, Henry O. Everitt, John M. Zavada, Tariq Manzur, Proc. of SPIE Vol. 8119, 81190A · © 2011 SPIE · CCC code: 0277-786X/11/$18 · doi: 10.1117/12.894223

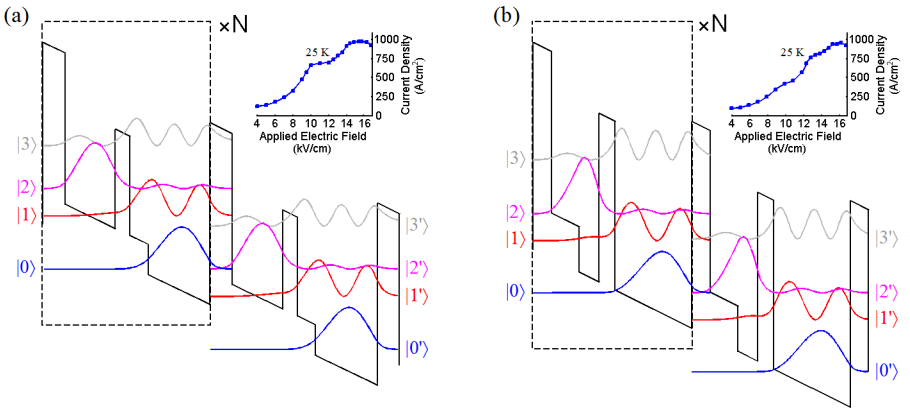

FIG. 1. (Color online) (a) Conduction band diagram showing the localized wavefunctions at an applied electric field of 15.5 kV/cm with one periodic section outlined. Beginning with the left injector, the $Al_xGa_{1-x}As$ layers compositions are 0.13/0.02/0.09/0.02/0 and thicknesses in nm are 4.8/11/3.2/4/13.5, with $\Delta E_{2\text{-}1}$ = 19.2 meV (~ 4.6 THz) and $\Delta E_{1\text{-}0}$ = 38 meV. (b) Conduction band diagram showing the localized wavefunctions at an applied electric field of 16.4 kV/cm with one periodic section outlined. Beginning with the left injector, the $Al_xGa_{1-x}As$ layers compositions are 0.15/0.03/0/0.12/0 and thicknesses in nm are 4/6.1/4.3/3.5/16.7, with $\Delta E_{2\text{-}1}$ = 19.4 meV (~ 4.7 THz) and $\Delta E_{1\text{-}0}$ = 37.3 meV. The center 2 nm of the last layer in each QC structure is assumed doped to a sheet density of 3.4×10^{10} cm^{-2}. The current density as a function of applied electric field bias found from the density matrix Monte Carlo simulations are shown inset for each structure.

fast intrawell electron-LO phonon scattering for depopulation that does not require resonant tunneling of the lower lasing state) while also improving the upper to lower lasing state LO phonon lifetime ratio $\tau_2/\tau_1 \sim 8$. These characteristics are desirable for any QC device and are the motivation for further investigating lattice temperature dependent properties of these structures. Diagonal optical transitions can and have been used to improve the injection selectivity in conventional square well QC structures, while at the same time usually also decreasing the oscillator strength.[3] With step well structures, good injection selectivity can be obtained somewhat more independent of the overlap of the optical transition wavefunctions.[19,20] A structure similar to that shown in Fig. 1b using square wells has been reported in Ref. 21.

In this paper, a density matrix Monte Carlo method is used to model the temperature effects in the step well QC structures shown in Fig. 1. The temperature dependent nonequilibrium electron distributions are solved and all states within a periodic section are modeled (including state $|3\rangle$). In this manner the intersubband scattering rates (including back-scatter rates) as well as all anticrossings are included in the analysis. Next, a brief description of the density matrix Monte Carlo method used to model the temperature dependent electron transport coherence and calculate the optical gain spectra in these structures will be described, and then the results from using this approach will be discussed.

2. ELECTRON TRANSPORT

To handle scattering between weakly coupled states as are present in QC structures, quantum coherence[22-25,4,9] is included in the transport analysis using density matrices similar to that described in Refs. 22-25. The density matrix Monte Carlo method has been previously used to model the electron transport in these step well structures at the cryogenic temperature of 25 K,[19] and this method is used in this paper to model lattice temperature effects. We additionally predict the temperature dependent optical gain spectra using what can be considered an extension to the simpler density matrix spectral approach used in Refs. 17 and 18. This allows the optical gain to be estimated without assuming a linewidth as a phenomenological parameter. Although this technique is used to model step well structures, it is valid for analyzing other types of QC structures as well.

2.1 Density matrix Monte Carlo method

In the density matrix Monte Carlo method transport coherence through the injector barrier is modeled using a density matrix approach including dephasing, while relaxation scattering is handled using a semiclassical Monte Carlo approach where the scattering rates are calculated via Fermi's golden rule.[4,9,19,26,27] Our specific implementation of the Monte Carlo portion of this simulation and the details of the scattering rate calculations have been previously described in Ref. 16, and the transport coherence implementation described in Ref. 19. Scattering mechanisms including electron-LO phonon, electron-electron, impurity, and interface roughness scattering are included in these calculations. Acoustic phonon scattering is not expected to contribute appreciably to the total scattering.[12] The nonequilibrium electron distributions are solved and used in the rate calculations and state blocking. No assumption or fitting to a Fermi-Dirac distribution is assumed. An effective electron temperature is used in the screening calculations. In our model, the temperature dependence enters from the occupation of the phonon modes and affects the electron distributions and screening. The density matrix method was implemented into the Monte Carlo simulation as follows. By including only coherent transport and dephasing the density operator equation becomes (with units of $\hbar = c = 1$)

$$\frac{\partial \rho_{ij}}{\partial t} = \sum \left(- L_{ij,mn} - T'^{-1} \delta_{im} \delta_{jn} \right) \rho_{mn}, \tag{1}$$

where $L_{ij,mn} = H_{im}\delta_{jn} - H^{*}_{jn}\delta_{im}$ is the Liouville operator which is a tetradic matrix and T' is the dephasing time used for all subbands. This equation is solved and used to describe the time evolution coherence of the electron ensemble without relaxation scattering. During the simulation relaxation scattering is handled in the usual Monte Carlo way, but the particle ensembles are no longer integer particles as they are in the case of an ensemble Monte Carlo simulation. Scattering events where the initial state population is scattered to a final state affect the diagonal elements as $\rho_{ii,\mathbf{k}_i} \rightarrow 0$ and $\rho_{ff,\mathbf{k}_f} \rightarrow |f\rangle\langle f|$. In order to take into account the ½ factor necessary for correctly calculating the total dephasing time (see below), when a scattering event occurs the off-diagonal $i \neq j$ elements are set to zero 50% of the time $\rho_{ij,\mathbf{k}_i}, \rho_{ji,\mathbf{k}_i} \rightarrow 0$ during the simulation.[9,19] Weighted averaging and *k*-space bins are used to keep from having an unbounded number of density matrices with different $\mathbf{k}_f$ values that would otherwise occur from these scattering events. A tight-binding method is used to calculate the localized basis wavefunctions that are used in these simulations.

2.2 Temperature dependent optical gain spectra

To calculate the optical gain spectra, the temperature dependent lifetimes solved from the transport model just described are used. An electric field perturbation is included of the form $\mathbf{E} = \boldsymbol{\mathcal{E}} \cos(\omega t)\,\hat{\mathbf{x}}$ incorporating the electric dipole interaction coherent coupling of the optical states. The time evolution of the density operator may now be written as

$$\begin{aligned} \frac{\partial \rho_{ij}}{\partial t} &= \sum \left[-iL'_{ij,mn} + W_{ji} - \left(W_{ji} + W_i \right) \delta_{ij} \right] \rho_{mn}, \qquad i = j \\ &= \sum \left\{ -iL'_{ij,mn} - \left[\frac{1}{2} \left(W_i + W_j \right) + T'_{ij} \right] \delta_{im} \delta_{jn} \right\} \rho_{mn}, \qquad i \neq j \end{aligned} \tag{2}$$

where $L'_{ij,mn} = H'_{im}\delta_{jn} - H'^{*}_{jn}\delta_{im}$, $H'_{ij} = H_{ij} + |e| x_{ul} \boldsymbol{\mathcal{E}} \cos(\omega t)\left(\delta_{iu}\delta_{jl} + \delta_{il}\delta_{ju} \right)$, $x_{ul} = \langle l | x | u \rangle$, u and l are the upper and lower lasing state indexes respectively, W_i is the total scattering rate out of state $|i\rangle$, W_{ji} is the scattering rate from $|j\rangle \rightarrow |i\rangle$, and T'_{ij} is the phenomenological or pure dephasing time between states $|i\rangle$ and $|j\rangle$. The total dephasing time τ_{deph} is related to the relaxation scattering time τ and T' by $\tau_{deph}^{-1} = ½\tau^{-1} + T'^{-1}$. The factor of ½ comes from the fact that $\rho_{ii} \propto |\rho_{ij}|^2$. The optical field Rabi frequency is $\Omega_{ul} = |e| x_{ul} \boldsymbol{\mathcal{E}} / \hbar$. The dynamics of the electron transport and optical coupling using the density matrix method are contained within and described by Eq. (2). The solution of the Eq. (2) allows for the electrical susceptibility $\chi = \chi' + i\chi''$ to be determined. The electrical susceptibility is found from the polarization **P** induced from the external optical field **E** and is $\chi(\omega) = -2|e| x_{ul} / \varepsilon V_c \boldsymbol{\mathcal{E}} \times \left[\rho_{ul}(\omega) + \rho_{lu}(-\omega) \right]$, where V_c is the volume of the resonant cavity. The optical gain can be calculated from

$$g(\omega) \cong \frac{k}{n_r^2} \chi''(\omega) \tag{3}$$

where k is the wave number and n_r is the index of refraction. In this manner, the density matrix Monte Carlo method along with Eqs. (2) and (3) allow for the temperature dependent optical gain spectrum to be calculated.

3. LATTICE TEMPERATURE SIMULATIONS

Since the electron transport of the two QC structures in Fig. 1 were previously modeled at the cryogenic lattice temperature of 25 K and found to have similar transport properties,[19] it was anticipated that their transport properties would also be similar at elevated lattice temperatures. The density matrix Monte Carlo method was used to find the subband populations as a function of lattice temperature (see Fig. 2), where a conservative dephasing time of $T' = 0.33$ psec was used in the simulations (corresponding to a linewidth of 4 meV prior to lifetime broadening $\approx 2\hbar/T'$). The two structures are seen to keep about the same population inversion over the temperature range from $T = 25$ to 300 K, where these calculations have been made at the design bias which is at the $|0\rangle \leftrightarrow |2'\rangle$ resonance. Also shown (as insets) in Fig. 2 are the electron distributions as well as the ratio of the population inversion to the total 2D population $\Delta n_{2\text{-}1}/n_{2D}$ for different dephasing times of $T' = 0.33$ and 0.5 psec. As expected, these graphs illustrate that the population inversion will increase with less pure dephasing scattering (corresponding to the larger $T' = 0.5$ psec). Since the two structures are indeed simulated to have similar temperature dependence, we next choose to calculate the optical gain spectra only for the structure in Fig. 1b. This structure was chosen since it was modeled to have slightly better isolation at the intermediate bias corresponding to where states $|0\rangle \leftrightarrow |1'\rangle$ become resonantly aligned (as can be seen from the inset current density curves, where a bump in the curve at ~ 10 kV/cm is noted for the QC structure in Fig. 1a).

The optical gain spectra for the Fig. 1b QC structure were computed for lattice temperatures from $T = 25$ to 250 K (in steps of $\Delta T = 25$ K) using the density matrix Monte Carlo method (see Fig. 3). The spectra shown in Fig. 3 were calculated in the weak optical field limit field limit $\mathcal{E} \rightarrow 0$ to illustrate the temperature dependent broadening in the absence of an optical field. A peak optical gain of ~ 80 cm^{-1} is calculated with a FWHM linewidth $\Delta\nu = 1.74$ THz at 25 K. The optical gain decreases relatively slowly out to about 100 K, due to these relatively low lattice temperatures and possibly the diagonally made optical transition. However, at elevated lattice temperatures above 100 K the maximum optical gain is calculated to decreases rapidly within increasing temperature due to the thermally active electron-LO phonon scattering. The linewidths are calculated to be fairly broad compared to some reported experimentally measured linewidths in different QC structures[28] and $T' = 0.33$ psec used in these calculations may be

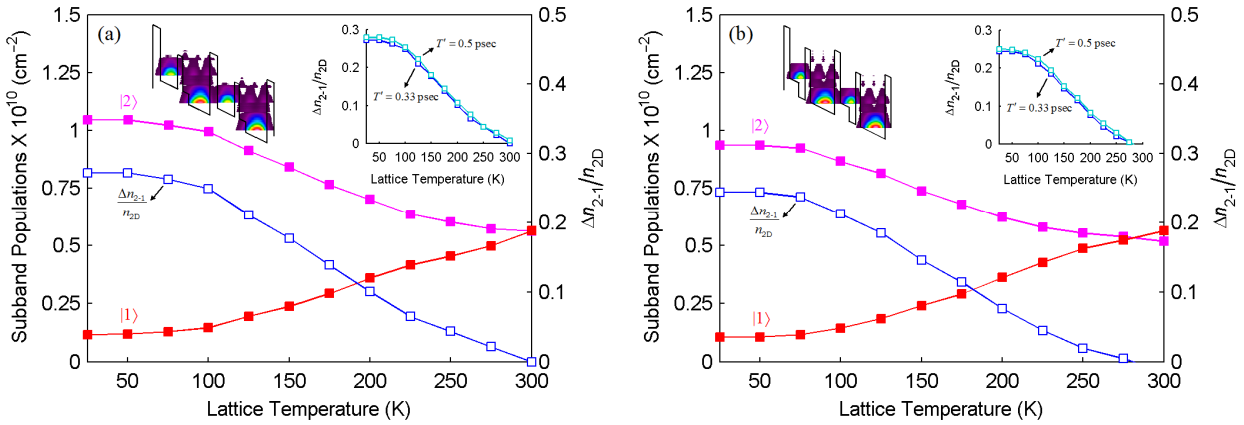

FIG. 2. (Color online) Results of the density matrix Monte Carlo simulations of the (a) Fig. 1a and (b) Fig. 1b QC structures. The population densities of the upper $|2\rangle$ and lower $|1\rangle$ lasing subbands as well as the ratio of the population inversion to the total 2D population $\Delta n_{2\text{-}1}/n_{2D}$ as a function of lattice temperature for $T' = 0.33$ psec. The state populations have been calculated at the $|0\rangle \leftrightarrow |2'\rangle$ resonance. Inset: The electron distributions for all subbands in each structure at $T = 25$ K (showing two periodic sections of the cascade) as well as $\Delta n_{2\text{-}1}/n_{2D}$ as a function of lattice temperature for $T' = 0.33$ and 0.5 psec.

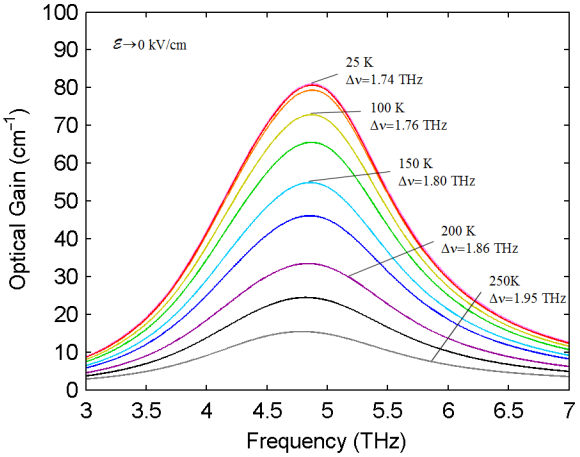

FIG. 3. (Color online) The optical gain spectra for the Fig. 1b QC structure for different lattice temperatures found from the density matrix Monte Carlo simulations. The spectra have been calculated at the $|0\rangle \leftrightarrow |2'\rangle$ resonance in the weak optical field limit $\mathcal{E} \rightarrow 0$. The values of the FWHM linewidths $\Delta\nu$ are indicated alongside various spectral curves.

somewhat short. Though spontaneous emission data has not been reported for many devices perhaps due to the difficulty in measuring sub-threshold spectra in low loss and low output coupling metal-metal waveguides.

To account for the optical field present in the resonant cavity, the optical gain spectra were calculated for different field strengths ranging from $\mathcal{E} \rightarrow 0$ to 4 kV/cm at lattice temperatures of T = 25, 100, and 200 K (see Fig. 4). These curves illustrate the effects of the optical field that are seen as both a reduction in the peak gain as well as an increase in the linewidth as expected. Relatively good optical gain was calculated at 100 K (shown inset in Fig. 4) even at relatively high optical field strengths ($g \sim 58$ cm^{-1} at T = 100 K and $\mathcal{E}$ = 3 kV/cm). At 200 K the peak optical gain was calculated ~ 33 cm^{-1} to below 20 cm^{-1} over the range of field strengths simulated (also shown inset in Fig. 4). Although modeling of metal-metal waveguide resonators using the finite element method has computed threshold gain values to be less than this[29,16] which suggests the possibility for device operation above 200 K, these models may be somewhat idealized. In

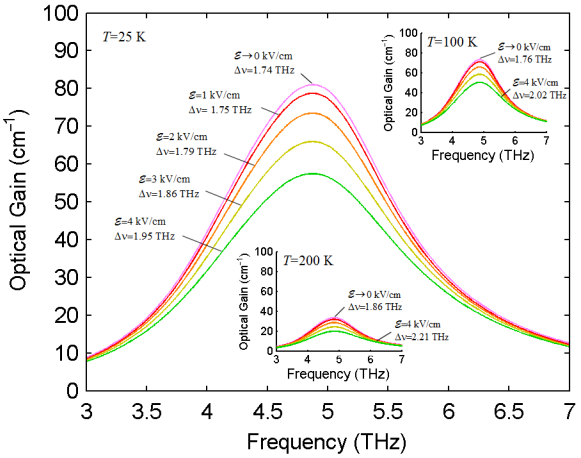

FIG. 4. (Color online) The optical gain spectra for the Fig. 1b QC structure for different optical electric field perturbation strengths at lattice temperatures of T = 25, 100, and 200 K (curves for T = 100 and 200 K are shown as insets) found from the density matrix Monte Carlo simulations. The spectra have been calculated at the $|0\rangle \leftrightarrow |2'\rangle$ resonance. The values of the FWHM linewidths $\Delta\nu$ are indicated alongside the spectral curves.

Ref. 30 the experimentally estimated threshold gain was ~ 36±10 cm^{-1} which indicates operation above 200 K unlikely. Even though these simulations have incorporated quantum coherence and a temperature dependent optical gain method which models all of the states within the QC structure, modeling all states as being localized could lead to optimistic predictions. Also, different temperature dependent screening models are possible. Thus, the optical gain at elevated lattice temperatures may be less than what has been calculated. Nevertheless, this study of structures that have characteristics favorable for elevated temperature operation (near unity injection efficiency, diagonal optical transition, and fast intrawell LO phonon scattering for depopulation) reiterates the findings of others[31] of the difficulty in obtaining elevated temperature operation in QC devices based on semiconductors with LO phonon energies close to the room temperature thermal energy $k_B T \sim 26$ meV such as in GaAs where $\hbar\omega_{LO} \sim 36$ meV.

4. CONCLUSIONS

An extension to the density matrix Monte Carlo method which allows for estimation of the temperature dependent optical gain spectra for QC devices has been presented. The maximum optical gain is calculated without assuming a linewidth, as both parameters are obtained from the computed optical gain spectrum. The optical field is also included in these calculations. This analysis contains only one phenomenological dephasing parameter. The nonequilibrium electron distributions are solved and this method is valid for modeling the electron transport in any type of QC structure. The step well structures investigated feature some useful characteristics for good temperature performance, yet still are predicted to have a maximum operating temperature on the order of ~ 200 K or perhaps somewhat lower. This reiterates the known difficulty of device operation at elevated lattice temperatures for GaAs semiconductor QC structures where the LO phonon energy is relatively small compared to the thermal energy.

ACKNOWLEDGEMENTS

This work is supported by ONR through the ILIR Program. One of us (GK) would also like to acknowledge the support from a NRO grant.

REFERENCES

[1] R. Köhler, A. Tredicucci, F. Beltram, H. E. Beere, E. H. Linfield, A. G. Davies, D. A. Ritchie, R. C. Iotti, and F. Rossi, "Terahertz semiconductor-heterostructure laser," Nature (London) **417**, 156 (2002).

[2] B. S. Williams, "Terahertz quantum-cascade lasers," Nature **1**, 517 (2007).

[3] S. Kumar, Q. Hu, and J. L. Reno, "186 K operation of terahertz quantum-cascade lasers based on a diagonal design," Appl. Phys. Lett. **94**, 131105 (2009).

[4] R. C. Iotti and F. Rossi, "Nature of charge transport in quantum-cascade lasers," Phys. Rev. Lett. **87**, 146603 (2001).

[5] R. Köhler, R. C. Iotti, A. Tredicucci, and F. Rossi, "Design and simulation of terahertz quantum cascade lasers," Appl. Phys. Lett. **79**, 3920 (2001).

[6] S.-C. Lee and A. Wacker, "Nonequilibrium Green's function theory for transport and gain properties of quantum cascade structures," Phys. Rev. B **66**, 245314 (2002).

[7] D. Indjin, P. Harrison, R. W. Kelsall, and Z. Ikonić, "Mechanisms of temperature performance degradation in terahertz quantum-cascade lasers," Appl. Phys. Lett. **82**, 1347 (2003).

[8] F. Banit, S.-C. Lee, A. Knorr, and A. Wacker, "Self-consistent theory of the gain linewidth for quantum-cascade lasers," Appl. Phys. Lett. **86**, 041108 (2005).

[9] H. Callebaut and Q. Hu, "Importance of coherence for electron transport in terahertz quantum cascade lasers," J. Appl. Phys. **98**, 104505 (2005).

[10] C. Jirauschek, G. Scarpa, P. Lugli, M. S. Vitiello, and G. Scamarcio, "Comparative analysis of resonant phonon THz quantum cascade lasers," J. Appl. Phys. **101**, 086109 (2007).

[11] S.-C. Lee, F. Banit, M. Woerner, and A. Wacker, "Quantum mechanical wavepacket transport in quantum cascade laser structures," Phys. Rev. B **73**, 245320 (2006).

[12] R. Nelander and A. Wacker, "Temperature dependence of the gain profile for terahertz quantum cascade lasers," Appl. Phys. Lett. **92**, 081102 (2008).
[13] T. Kubis, C. Yeh, P. Vogl, A. Benz, G. Fasching, and C. Deutsch, "Theory of nonequilibrium quantum transport and energy dissipation in terahertz quantum cascade lasers," Phys. Rev. B **79**, 195323 (2009).
[14] T. Schmielau and M. F. Pereira, "Nonequilibrium many body theory for quantum transport in terahertz quantum cascade lasers," Appl. Phys. Lett. **95**, 231111 (2009).
[15] R. Nelander and A. Wacker, "Temperature dependence and screening models in quantum cascade structures," J. Appl. Phys. **106**, 063115 (2009).
[16] W. Freeman and G. Karunasiri, "Monte Carlo simulation of step well quantum cascade laser structures," Proc. SPIE, **7311**, 7311V (2009).
[17] S. Kumar and Q. Hu, "Coherence of resonant-tunneling transport in terahertz quantum-cascade lasers," Phys. Rev. B **80**, 245316 (2009).
[18] E. Dupont, S. Fathololoumi, and H. C. Liu, "Simplified density-matrix model applied to three-well terahertz quantum cascade lasers," Phys. Rev. B **81** 205311 (2010).
[19] W. Freeman, "Modeling electron transport coherence in one and two-well terahertz step well quantum cascade structures with diagonal optical transitions," Proc. SPIE **8023**, 802305 (2011).
[20] W. Freeman and G. Karunasiri, "Proposed use of step quantum wells for terahertz quantum cascade lasers," Proc. Ninth Int. Conf. on Intersubband Transitions in Quantum Wells, (2007), http://www.itqw07.leeds.ac.uk/abs/.
[21] S. Kumar, C. W. I. Chan, Q. Hu, and J. L. Reno, "Two-well terahertz quantum-cascade laser with direct intrawell-phonon depopulation," Appl. Phys. Lett. **95**, 141110 (2009).
[22] R. F. Kazarinov and R. A. Suris, "Possibility for the amplification of electromagnetic waves in a semiconductor with a superlattice," Sov. Phys. Semicond. **5**, 707 (1971).
[23] R. F. Kazarinov and R. A. Suris, "Electric and electromagnetic properties of semiconductors with a superlattice," Sov. Phys. Semicond. **6**, 120 (1972).
[24] S. Mukamel, *Principles of Nonlinear Optical Spectroscopy*, Oxford University Press, New York (1995).
[25] C. Sirtori, F. Capasso, J. Faist, A. L. Hutchinson, D. L. Sivco, and A. Y. Cho, "Resonant tunneling in quantum cascade lasers," IEEE J. Quantum Electron. **34**, 1722 (1998).
[26] H. D. Rees, "Calculation of steady state distribution functions by exploiting stability," Phys. Lett. **26A**, 416 (1968).
[27] C. Jacoboni and L. Reggiani, "The Monte Carlo method for the solution of charge transport in semiconductors with applications to covalent materials," Reviews of Modern Physics **55**, 645 (1983).
[28] N. Jukam, S. S. Dhillon, D. Oustinov, J. Madéo, J. Tignon, R. Colombelli, P. Dean, M. Salih, S. P. Khanna, E. H. Linfield, and A. G. Davies, "Terahertz time domain spectroscopy of phonon-depopulation based quantum cascade lasers," Appl. Phys. Lett. **94**, 251108 (2009).
[29] S. Kohen, B. S. Williams, and Q. Hu, "Electromagnetic modeling of terahertz quantum cascade laser waveguides and resonators," J. Appl. Phys. **97**, 053106 (2005).
[30] L.A. Dunbar, R. Houdré, G. Scalari, L. Sirigu, M. Giovannini, and J. Faist, "Small optical volume terahertz emitting microdisk quantum cascade laser," Appl. Phys. Lett. **90**, 14114 (2007).
[31] E. Bellotti, K. Driscoll, T. D. Moustakas, and R. Paiella, "Monte Carlo Study of GaN versus GaAs terahertz quantum cascade structures," Appl. Phys. Lett. **92**, 101112 (2008).